Biophysical Journal Volume 105 November 2013 2006–2015

Effects of Intercellular Junction Protein Expression on Intracellular Ice Formation in Mouse Insulinoma Cells

Adam Z. Higgins[†] and Jens O. M. Karlsson[‡*]

[†]School of Chemical, Biological and Environmental Engineering, Oregon State University, Corvallis, Oregon; and [‡]Department of Mechanical Engineering, Villanova University, Villanova, Pennsylvania

ABSTRACT The development of cryopreservation procedures for tissues has proven to be difficult in part because cells within tissue are more susceptible to intracellular ice formation (IIF) than are isolated cells. In particular, previous studies suggest that cell-cell interactions increase the likelihood of IIF by enabling propagation of ice between neighboring cells, a process thought to be mediated by gap junction channels. In this study, we investigated the effects of cell-cell interactions on IIF using three genetically modified strains of the mouse insulinoma cell line MIN6, each of which expressed key intercellular junction proteins (connexin-36, E-cadherin, and occludin) at different levels. High-speed video cryomicroscopy was used to visualize the freezing process in pairs of adherent cells, revealing that the initial IIF event in a given cell pair was correlated with a hitherto unrecognized precursor phenomenon: penetration of extracellular ice into paracellular spaces at the cell-cell interface. Such paracellular ice penetration occurred in the majority of cell pairs observed, and typically preceded and colocalized with the IIF initiation events. Paracellular ice penetration was generally not observed at temperatures $>-5.65^{\circ}C$, which is consistent with a penetration mechanism via defects in tight-junction barriers at the cell-cell interface. Although the maximum temperature of paracellular penetration was similar for all four cell strains, genetically modified cells exhibited a significantly higher frequency of ice penetration and a higher mean IIF temperature than did wild-type cells. A four-state Markov chain model was used to quantify the rate constants of the paracellular ice penetration process, the penetration-associated IIF initiation process, and the intercellular ice propagation process. In the initial stages of freezing ($>-15^{\circ}C$), junction protein expression appeared to only have a modest effect on the kinetics of propagative IIF, and even cell strains lacking the gap junction protein connexin-36 exhibited nonnegligible ice propagation rates.

INTRODUCTION

The ability to store living tissue in the cryopreserved state would enable efficient mass-production of tissue engineered products (1) and facilitate transplantation procedures, especially when tissue from multiple donors must be pooled to achieve a minimum therapeutic dose (2). However, although suspended cells of various types can be successfully cryopreserved, cryopreservation of tissue has proven to be more difficult (1,3–7). This discrepancy may be related to differences in the likelihood of intracellular ice formation (IIF), a major mode of cryoinjury (1). In particular, the probability of IIF has been shown to be lower for suspended cells than for cell monolayers (8,9), suggesting that the latter are more susceptible to damage during the freezing process.

Stott and Karlsson (10) have recently investigated the effects of cell-substrate interactions on the freezing of adherent endothelial cells, using a high-speed video cryomicroscopy system. Observation of the freezing of micropatterned single-cell constructs at submillisecond temporal resolution revealed two new IIF initiation mechanisms unique to adherent cells (10). The term "peripheral-zone initiation" was used to describe a mode of IIF in which the intracellular crystal started growing at the distal edge of the spreading cell (10). A second mechanism of IIF discovered by Stott and Karlsson (10) was associated with a precursor phenomenon termed "paracellular ice penetration" (PIP), the growth of extracellular ice crystal protrusions into paracellular spaces that contain supercooled liquid. Because PIP and peripheral-zone initiation of IIF are associated with cell-substrate interactions, and do not occur during freezing of suspended cells, these mechanisms may contribute to the observed increase in IIF probability during freezing of tissue constructs. In addition to effects of cell-substrate interactions, cell-cell interactions in multicellular constructs have been shown to further enhance the probability of IIF (9).

The promotion of IIF by cell-cell interactions has been hypothesized to result from an ability of intracellular ice to propagate between neighboring cells. The early evidence for such intercellular ice propagation was derived from anecdotal observations of nonrandom spatial patterns of IIF, which suggested that internal ice could spread to neighboring cells (8,11–14). More recently, Irimia and Karlsson provided quantitative evidence for intercellular ice propagation by analyzing the freezing behavior of micropatterned cell pairs (9) and linear cell arrays (15). Intercellular ice

Submitted August 3, 2013, and accepted for publication September 16, 2013.

*Correspondence: karlsson@alum.mit.edu

Editor: Jeffrey Fredberg.

0006-3495/13/11/2006/10 $2.00

http://dx.doi.org/10.1016/j.bpj.2013.09.028

propagation has been suggested to result from ice growth through gap junction channels (13,14), and evidence supporting this hypothesis was obtained by Irimia and Karlsson, who demonstrated that the rate of propagation was significantly depressed after treatment with a gap junction inhibitor (9).

The objective of this study was to clarify the role of cell-cell interactions in IIF. In particular, we hypothesized that the level of expression of connexins and other intercellular junction proteins would affect the rate of ice propagation between neighboring cells. To test this hypothesis, we studied the freezing process in pairs of adherent mouse insulinoma cells, which had been genetically modified to express different levels of proteins required for the formation of gap junctions, adherens junctions, and tight junctions (16,17). Our high-speed video cryomicroscopy experiments revealed that IIF in adherent pairs of MIN6 cells appeared to be associated with PIP events at the cell-cell interface. Based on these observations, we developed a theoretical model of the freezing process, and used our model to quantify the effects of intercellular junction protein expression on the kinetics of the PIP process as well as the subsequent IIF kinetics.

THEORETICAL BACKGROUND

As explained in the Discussion, our experimental results suggest that IIF in tissue is mediated by paracellular penetration of extracellular ice into compartments at the interface between adjoining cells. Thus, to analyze our cryomicroscopy data, we modified the stochastic model of Irimia and Karlsson (9) to account for this PIP phenomenon.

Irimia and Karlsson (9) described the freezing kinetics of a cell pair using a continuous-time Markov chain model with three possible states for the cell pair:

1. State 0, the completely unfrozen state;
2. State 1, the singlet state, in which the pair comprises one frozen and one unfrozen cell; and
3. State 2, the doublet state, in which both cells in the pair are frozen.

The probabilities of these three states within an ensemble of cell pairs are p_0, p_1, and p_2, respectively, the evolution of which can be predicted by solving a Kolmogorov differential equation with a generator matrix that holds the transition intensities of each state transition process (9).

As shown in Fig. 1, we have modified the model of Irimia and Karlsson (9) by introducing an activated state (State 0*) between the unfrozen state and the singlet state, to represent PIP at the cell-cell interface. Thus, the intensity of the state transition $0 \rightarrow 0^*$ ($j_{0,0^*}$) is equal to J_{PIP}, the average rate of PIP per unfrozen cell pair. Following Irimia and Karlsson (9), we classify IIF mechanisms as either independent of, or dependent on, the state of IIF in the neighboring cell; the latter class represents intercellular ice propagation

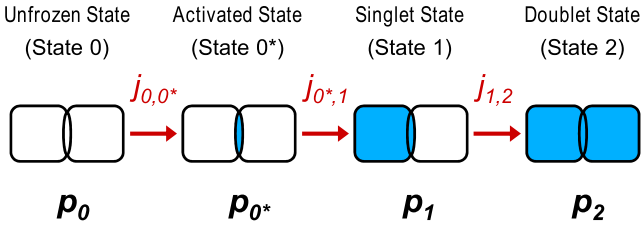

FIGURE 1 Markov chain model of proposed IIF mechanisms in a cell pair, showing the four states and associated state probabilities, as well as the possible state transition pathways and associated transition intensities. The cell pair schematic depicts two adjoining cells (drawn as *squares*) with a paracellular space at the cell-cell interface (drawn as a *thin ellipse*); open shapes represent unfrozen liquid; whereas solid shapes represent frozen domains.

events. Therefore, the transition intensity of the singlet formation reaction is given by $j_{0^*,1} = 2J_i$, where J_i is the average rate of cell-cell-interaction-independent IIF per unfrozen cell (9). Likewise, the doublet formation intensity is $j_{1,2} = J_i + J_p$, where J_p is the average rate of intercellular ice propagation per singlet (9). The modified Kolmogorov differential equation includes the probability p_{0^*} of the activated state, and becomes

$$\frac{d}{dt}\begin{bmatrix} p_0 \\ p_{0^*} \\ p_1 \\ p_2 \end{bmatrix} = \begin{bmatrix} -J_{\mathrm{PIP}} & 0 & 0 & 0 \\ J_{\mathrm{PIP}} & -2J_i & 0 & 0 \\ 0 & 2J_i & -(J_i + J_p) & 0 \\ 0 & 0 & J_i + J_p & 0 \end{bmatrix} \begin{bmatrix} p_0 \\ p_{0^*} \\ p_1 \\ p_2 \end{bmatrix} \tag{1}$$

The model in Eq. 1 becomes equivalent to the original three-state model by Irimia and Karlsson (9) in the regime $J_{\mathrm{PIP}} >> J_i$. An analysis of the solutions to Eq. 1 is provided in the Supporting Material.

To quantify the kinetics of a given state transition $a \rightarrow b$, it is convenient to define the corresponding cumulative intensity function,

$$N_{a,b}(t) \equiv \int_0^t j_{a,b}(\tau)\, d\tau \tag{2}$$

where $j_{a,b}$ is the transition intensity, and τ is the integration variable. Similarly, the cumulative hazards of PIP (N_{PIP}), cell-cell-interaction-independent IIF (N_i), and propagative IIF (N_p) are defined as the time-integrals of the rate coefficients J_{PIP}, J_i, and J_p, respectively. It can be shown that the mechanism-specific cumulative hazard functions are dependent on the cumulative intensities of the observable phase transition events as follows:

$$\begin{aligned} N_{\mathrm{PIP}} &= N_{0,0^*} \\ N_i &= \tfrac{1}{2} N_{0^*,1} \\ N_p &= N_{1,2} - \tfrac{1}{2} N_{0^*,1} \end{aligned} \tag{3}$$

Thus, if the cumulative intensity functions $N_{a,b}(t)$ are known, it is possible to determine the magnitude of the rate constants J_{PIP}, J_i, and J_p by estimating the time-derivates of the quantities computed in Eq. 3.

MATERIALS AND METHODS

Cell lines

Experiments were performed using wild-type MIN6 cells and three different genetically modified strains, allowing a systematic evaluation of the effects of intercellular junction protein expression on the IIF process. Wild-type MIN6 cells (18) are known to express several intercellular junction proteins, including the gap junction protein connexin-36, the adherens junction protein E-cadherin, and the tight junction protein occludin (16,17). To create the genetically modified cell lines, Calabrese et al. (16) first stably transfected wild-type cells with antisense RNA for connexin-36. Calabrese et al. (17) characterized these antisense-transfected cells using a panel of Western blots for intercellular junction proteins, revealing significantly reduced expression of connexin-36, but also a significant downregulation of E-cadherin and occludin. Calabrese et al. (17) therefore rescued the antisense-transfected strain by restoring expression of either connexin-36 or E-cadherin to normal levels. Thus, the four MIN6 strains are: wild-type; antisense-transfected cells (AS); antisense-transfected strain with restored connexin-36 expression (AS+Cx); and antisense-transfected strain with restored E-cadherin expression (AS+Ecad). The known properties of the cell lines used in this study are summarized in Table 1.

Cell culture

All MIN6 strains were generously provided by Dr. Paolo Meda (University of Geneva, Geneva, Switzerland). Cells were cultured on tissue-culture-treated plastic in high-glucose Dulbecco's Modified Eagle's Medium (Invitrogen, Carlsbad, CA), which had been supplemented with 15% (v/v) heat-inactivated fetal bovine serum (Sigma-Aldrich, Saint Louis, MO) and 0.07 mM β-mercaptoethanol (Invitrogen), and were maintained at 37°C in a 5% CO_2 environment. Media were changed every 3 days and passages were performed weekly. To harvest cells for sample preparation or culture passage, cell monolayers were digested by exposure to 0.024% (w/v) trypsin for 5 min.

Sample preparation

For cryomicroscopy experiments, harvested MIN6 cells were seeded at a density of ~10^5 cells/cm^2 onto 12-mm diameter glass coverslips in petri dishes and subsequently cultured for 48 h. These coverslips were then transferred into a fluorescence staining medium consisting of 2 μM SYTO13 (a membrane-permeable nucleic acid stain; Molecular Probes, Eugene, OR) and 2 μM ethidium homodimer-1 (a membrane impermeable nucleic acid stain; Molecular Probes) in culture medium and incubated at 37°C for 10–60 min. Immediately before freezing, the samples were removed from the staining medium, rinsed with isotonic phosphate-buffered saline (with Ca^{2+} and Mg^{2+}; Mediatech, Manassas, VA), and inverted onto a 16-mm coverslip, creating a coverslip sandwich with the adherent cells in the middle.

TABLE 1 Intercellular junction protein expression in the MIN6 cell lines

Protein	Wild-Type	AS	AS+Ecad	AS+Cx	References
Connexin-36	+	−	−	+	(16,17)
E-cadherin	+	−	+	−	(17)
Occludin	+	−	−	−	(17)

Cryomicroscopy

Our high-speed video cryomicroscopy system has been described previously (10). It consists of a microscope (Eclipse ME600; Nikon, Tokyo, Japan), a temperature-controlled microscope stage (FDCS-196; Linkam Scientific Instruments, Tadworth, Surrey, United Kingdom), and a high-speed video camera (Phantom v4.3; Vision Research, Wayne, NJ). After loading a sample into the cryomicroscope stage chamber, it was first cooled to −2°C at 50°C/min and held at this temperature for 1 min. During this time period, the sample was brought into contact with a cold-spot built into the cryomicroscope stage, to initiate formation of extracellular ice. The sample was then heated to −1.5°C at 10°C/min and held at this temperature for ~90 s, during which time a field of view was randomly selected that contained a single cell pair (as determined by visualization of two distinct nuclei using SYTO13 fluorescence) with intact cell membranes (as determined by lack of ethidium homodimer-1 fluorescence). The sample was then cooled rapidly to −60°C at 130°C/min. During this rapid cooling process, images were acquired at a sampling rate of 3000–4000 Hz, enabling visualization of the intracellular ice growth process, which manifested as a directional wave with a timescale of ~3 ms (10). IIF locations were classified into three groups: cell-cell interface; perimeter (of the cell-substrate contact area); or interior. In some cases extracellular ice obscured the cells, preventing unambiguous identification of the location of IIF initiation. These cell pairs were excluded from analysis of the IIF location. PIP was identified as a sudden darkening at the cell-cell interface, with a timescale of the order of ~100 ms. The cumulative IIF probability was determined from the cryomicroscopy data by dividing the number of frozen cells by the total number of cells. In addition, the time and temperature associated with the state transitions illustrated in Fig. 1 were determined for each video recording.

Statistical analysis

Unless otherwise noted, experimental data are reported as averages and standard error of the mean. For normally distributed data and equal variances, the data were analyzed by analysis of variance (ANOVA), followed by Tukey's tests. When data were nonnormal or groups had unequal variances, the data were analyzed using a nonparametric Kruskal-Wallis ANOVA, followed by Dunn's method for pairwise comparisons. For frequency data resulting from classification of events into categories (i.e., IIF location, incidence of PIP), the standard deviation was estimated as the square-root of the number of observations in each category, as expected for a Poisson process. Such categorical frequency data were analyzed using χ^2 tests. For comparison of the slopes of best-fit lines, a two-tailed t-test was used. Differences were considered to be significant at a confidence level of 95% ($p < 0.05$).

The cumulative hazards of PIP, cell-cell-interaction-independent IIF, and intercellular ice propagation were determined from Eq. 3, using estimates of the cumulative intensity functions $N_{a,b}(t)$. For each state transition $a \rightarrow b$ depicted in Fig. 1, $N_{a,b}(t)$ was estimated from experimental observations of the corresponding event in an ensemble of cell pairs. In particular, we used a modified form (19) of the Nelson-Aalen estimator (20,21) for multiplicative intensity models, as follows:

$$N_{a,b}(t) = \frac{1}{2}\sum_{k=1}^{M_{a,b}(t)}\left(\frac{1}{n_a(t_k^-)} + \frac{1}{n_a(t_k^+)}\right) \tag{4}$$

where $M_{a,b}(t)$ is the total number of state transitions $a \rightarrow b$ that have been observed at time t; $n_a(t)$ is the total number of cell pairs found in state a (i.e., the risk group) at time t; t_k represents the time of the kth state transition

event of type $a \rightarrow b$; and the superscript signs indicate left-hand ($-$) and right-hand ($+$) limits, respectively.

RESULTS

Effect of intercellular junction protein expression on IIF initiation

The cumulative IIF probability is shown in Fig. 2 *A* for each of the MIN6 strains. These data represent the combined effects of all IIF mechanisms. As shown in Fig. 2 *A*, the wild-type cells exhibited a cumulative IIF probability distribution different from the trends that were observed for each of the genetically modified strains. In particular, wild-type cells underwent IIF at a significantly lower temperature ($-23.2 \pm 0.4°C$, $p < 0.05$) than did AS, AS+Ecad, and AS+Cx cells ($-14.6 \pm 0.3°C$, $-13.2 \pm 0.4°C$, and $-13.0 \pm 0.4°C$, respectively). To further characterize the effect of the genetic modifications on IIF, we determined the probability of the initial IIF event (i.e., formation of the singlet state) during freezing of ensembles of MIN6 cell pairs. As shown in Fig. 2 *B*, the mean temperature of the initial IIF event was significantly lower in wild-type cells ($-22.5 \pm 0.6°C$, $p < 0.05$) than in the genetically modified clones ($-14.0 \pm 0.4°C$, $-12.1 \pm 0.5°C$, and $-12.3 \pm 0.5°C$ for AS, AS+Ecad, and AS+Cx, respectively). Because the initial IIF event is not dependent on intercellular ice propagation (9,15), the results in Fig. 2 *B* indicate that the effects of intercellular junction protein expression on IIF kinetics (Fig. 2 *A*) cannot be entirely attributed to differences in propagation kinetics, as originally hypothesized.

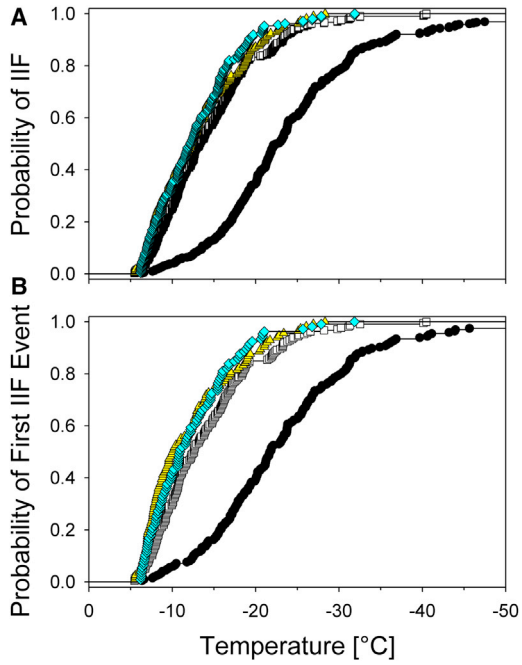

FIGURE 2 (*A*) Cumulative overall probability of IIF and (*B*) cumulative probability of the initial IIF event in each cell pair during rapid cooling to $-60°C$. Data are shown for observations of 196 pairs of wild-type cells (*circles*), 213 AS pairs (*squares*), 114 AS+Ecad pairs (*triangles*), and 106 AS+Cx pairs (*diamonds*).

Paracellular ice penetration at the cell-cell interface

To explore the reasons for the differences in the kinetics of IIF initiation, we examined, in slow-motion playback, high-speed video recordings of the time interval preceding the first incidence of IIF in each cell pair. In a majority of videos (>70%), we observed sequential darkening of multiple small (~1 μm) domains located along the interface of the two adjoining cells. Such interfacial darkening sequences progressed over a timescale of ~100 ms (whereas each individual darkening event was <10 ms in duration), and appeared to frequently precede and colocalize with the subsequent IIF initiation events. For example, in the representative cryomicroscopy video shown in Movie S1 in the Supporting Material (see Fig. 3 for corresponding still images), multiple microscale darkening events can be seen at the cell-cell interface over an 80-ms interval, starting when the temperature reached $-14.8°C$ (Fig. 3, *A–C*). Shortly afterward, in one of the cells, IIF manifested as an advancing semicircular solidification front with an origin at the darkened cell-cell interface (Fig. 3 *D*; also see Movie S2). This was followed by IIF in the second cell, manifesting again as an advancing ice front with an initiation site at the darkened portion of the cell-cell interface (Fig. 3 *E*; also see Movie S3). As explained in the Theoretical Background and in the Discussion, we have hypothesized that the IIF precursor events observed at the cell-cell interface represent a form of paracellular ice penetration, a phenomenon previously described by Stott and Karlsson (10). Thus, hereinafter we will use this terminology (PIP) to describe the interfacial darkening events observed in MIN6 cell pairs.

To determine the prevalence of paracellular ice penetration during freezing of MIN6 cell pairs to $-60°C$, we systematically reviewed ~100 cryomicroscopy videos for each of the four MIN6 strains. In the wild-type strain, PIP occurred in 47% of cell pairs, whereas 79% of cell pairs from the AS strain exhibited PIP; the frequency of PIP in the AS+Ecad and AS+Cx strains was even higher (91 and 84%, respectively). A χ^2 analysis of the entire data set revealed that the effect of intercellular junction protein expression on the incidence of PIP was statistically significant ($p < 0.001$). In pairwise comparisons, each of the genetically modified MIN6 strains was found to have a significantly higher incidence of PIP than did wild-type cells ($p < 0.001$). The incidence of PIP was also higher for AS+Ecad cells than for the AS strain ($p < 0.05$).

To quantify the kinetics of PIP, we analyzed the transition between the unfrozen and activated states (see Fig. 1) using Eqs. 3–4. The resulting cumulative hazard of PIP is plotted in Fig. 4. With the exception of some scatter in the low-temperature data for the AS+Cx group, all MIN6

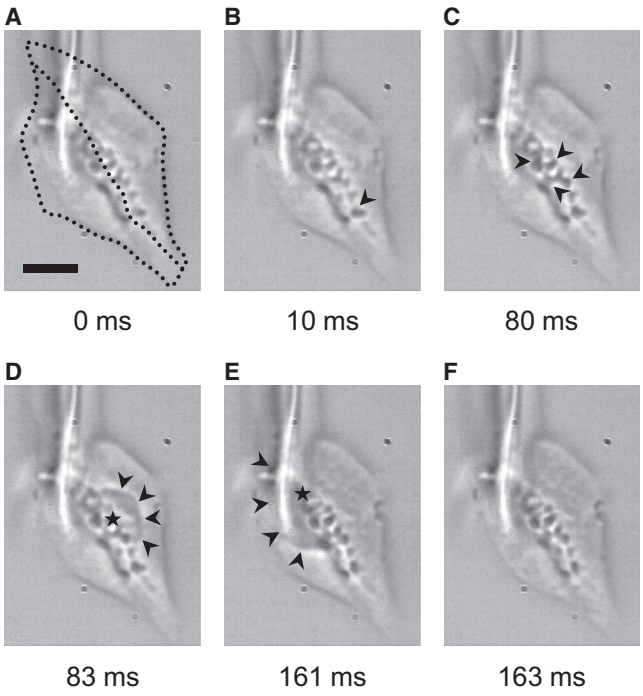

FIGURE 3 Still images from a high-speed video recording that depicts the freezing of a MIN6-AS cell pair; slow-motion playback of the full video can be seen in Movie S1 in the Supporting Material. (*A*) Video frame acquired at −14.8°C, just before paracellular and intracellular freezing events. Dotted lines mark the cell boundaries; scale bar: 10 μm. (*B*) Initial manifestation of paracellular ice penetration; arrowhead marks the location of the first darkening event at the cell-cell interface. (*C*) Continuation of the paracellular ice penetration process, comprising multiple localized darkening events at the cell-cell interface (*arrowheads*). (*D*) Initial IIF event, manifesting as a solidification front (*arrowheads*) advancing from an initiation site at the cell-cell interface (*asterisk*); slow-motion video of this event is shown in Movie S2. (*E*) IIF in the second cell, with the associated solidification front (*arrowheads*) also originating from a site at the cell-cell interface (*asterisk*); the corresponding video is shown in Movie S3. (*F*) Completion of the IIF process, at −15.1°C. All time stamps are relative to the initial video frame (*A*).

variants exhibited approximately linear trends in N_{PIP} at temperatures <-6°C, indicating that the magnitude of the rate J_{PIP} undergoes a step change upon reaching this temperature. Linear regression of the data between −6 and −12°C yielded best-fit PIP rates of 0.111 ± 0.004 s^{-1} for wild-type cells, 0.466 ± 0.006 s^{-1} for AS cells, 0.850 ± 0.008 s^{-1} for AS+Ecad cells, and 0.609 ± 0.007 s^{-1} for AS+Cx cells. All pairwise comparisons of slopes yielded differences that were statistically significant ($p < 0.001$). In contrast, all linear regressions intercepted the time-axis ($N_{PIP} = 0$) at approximately the same temperature, representing an extrapolated maximum temperature for PIP (T_{PIP}^{max}). Specifically, the intercepts were $T_{PIP}^{max} = -5.69$°C for wild-type cells, with a 95% confidence interval (CI) from −5.92 to −5.43°C; $T_{PIP}^{max} = -5.77$°C (CI: −5.84 to −5.69°C) for the AS strain; $T_{PIP}^{max} = -5.66$°C (CI: −5.71 to −5.62°C) for the AS+Ecad strain; and $T_{PIP}^{max} = -5.48$°C (CI: −5.54 to −5.41°C) for the AS+Cx strain. Thus, the average intercept value (−5.65°C) can be taken as an approximate upper bound, above which PIP is (generally) not observed in any of the MIN6 strains.

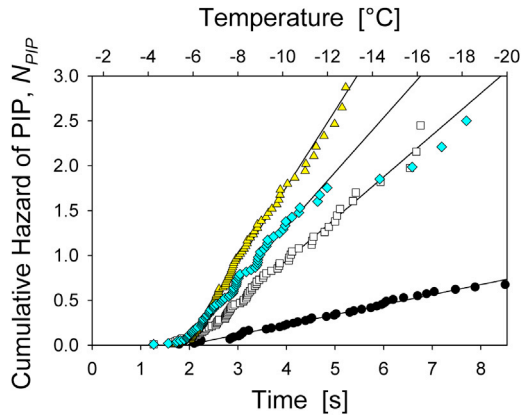

FIGURE 4 Estimated cumulative hazard of PIP (N_{PIP}) for cell pairs consisting of wild-type (*circles*), AS (*squares*), AS+Ecad (*triangles*), or AS+Cx strains of MIN6 (*diamonds*). Solid lines represent linear fits to data in the temperature range −6 to −12°C.

Correlation between PIP and IIF

The relative magnitude of the rates of PIP for the four groups (shown in Fig. 4) is consistent with the trend in mean temperatures of the first IIF event in paired MIN6 cells (i.e., wild-type < AS < AS+Cx < AS+Ecad), as shown in Fig. 2 *B*. This is significant because the first IIF event in a cell pair is, by definition, independent of intercellular ice propagation, so the probability of the first IIF event is a function of the cell-cell-interaction-independent rate process (J_i), as shown in Fig. 1. Therefore, the correlation observed above suggests that PIP may play a role in the cell-cell-interaction-independent mechanism of IIF.

To further characterize the apparent correlation between PIP and IIF, we examined the spatial distribution of IIF initiation sites for the singlet formation events (i.e., state transition $0^* \rightarrow 1$ in Fig. 1). As shown in Fig. 5 *A*, the majority of such IIF initiation sites were located at the cell-cell interface. For cell pairs constructed from any of the four MIN6 cell variants, the proportion of initial IIF events that originated from the cell-cell interface was significantly higher than the proportion of initial IIF events that originated from either the cell perimeter or the cell interior ($p < 0.001$). Because all PIP events observed in adherent MIN6 pairs also occurred at the cell-cell interface, these data demonstrate that the cell-cell-interaction-independent mechanism of IIF (J_i) is spatially correlated with the PIP process.

A temporal association between PIP and cell-cell-interaction-independent IIF was also verified, as illustrated by correlating the temperatures of PIP and the initial IIF events in each cell pair (Fig. 5 *B*); because experiments were conducted using a constant rate of cooling, a correlation

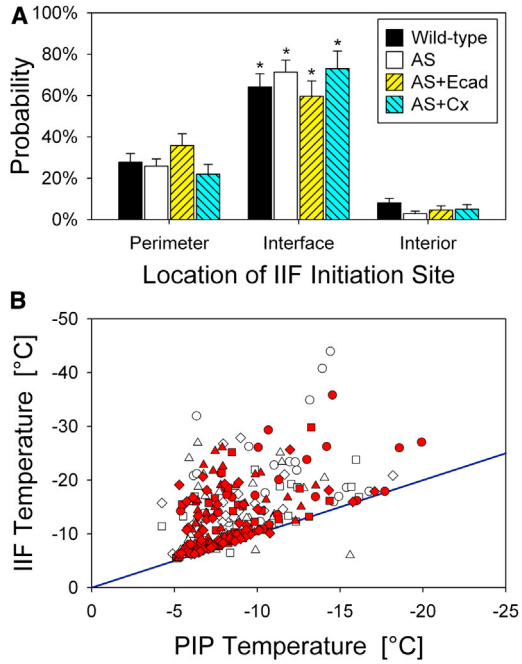

FIGURE 5 Evidence for correlation between PIP event at cell-cell interface and the first IIF event in cell pairs consisting of various MIN6 strains. (*A*) Spatial distribution of IIF initiation sites, categorized as located either on the perimeter (i.e., the outer boundary of the substrate area occupied by the adherent cell pair), on the cell-cell interface, or in the interior (i.e., inside the projected cell boundaries). Asterisks indicate significantly higher incidence of IIF initiation at the cell-cell interface than at the other IIF initiation sites ($p < 0.001$). (*B*) Correlation between temperatures of PIP and the initial IIF event for cell pairs consisting of wild-type (*circles*), AS (*squares*), AS+Ecad (*triangles*), or AS+Cx strains (*diamonds*); solid symbols indicate IIF events that originated at the cell-cell interface. The solid line has unity slope, representing the hypothetical case of concurrent PIP and IIF (i.e., for data points located above this line, IIF occurred after the PIP event).

of temperatures is equivalent to a temporal correlation. Linear regression of the data sets in Fig. 5 *B* (not shown) yielded slopes that were significantly greater than zero for all of the MIN6 cell variants ($p < 0.03$), indicating that the temperatures (and hence, times) of IIF and PIP are correlated. Furthermore, PIP preceded IIF in >97% of cell pairs observed: the average time delay between PIP and the first IIF event was 4.5 ± 0.5 s, 1.6 ± 0.2 s, 2.0 ± 0.2 s, and 1.8 ± 0.2 s for wild-type, AS, AS+Ecad, and AS+Cx, respectively, each of which is significantly greater than zero ($p < 0.001$). We recognize the possibility of selection bias due to the fact that high-speed video recordings were terminated shortly after observation of IIF (thus reducing the opportunity to observe PIP events that may have occurred after IIF). Nonetheless, the average length of video recording after the first IIF event was 3.2 s, whereas the average length of video recording before IIF was 14.4 s. Thus, if PIP and IIF events were uncorrelated, 18% of the video recordings should include PIP events that occurred after IIF; in contrast, PIP was observed after IIF in only ~2% of the experiments. Therefore, it is unlikely that the observed temporal correlation between PIP and IIF was due to sampling bias ($p < 0.0001$).

Effect of intercellular junctions on PIP-associated IIF initiation

As shown in Fig. 6, we determined the rate of PIP-associated independent IIF (J_i) by linear regression of the corresponding cumulative hazard, which was estimated by analyzing transitions from the activated state to the singlet state ($0^* \rightarrow 1$, see Fig. 1) using Eqs. 3–4. Based on the slope in the temperature interval from −6 to −25°C, the rate of the PIP-associated independent IIF process was highest for AS cells ($J_i = 0.299 \pm 0.008\ s^{-1}$), and lowest for wild-type cells ($J_i = 0.093 \pm 0.005\ s^{-1}$). Intermediate values of $J_i = 0.198 \pm 0.004\ s^{-1}$ and $J_i = 0.265 \pm 0.005\ s^{-1}$ were observed for AS+Ecad and AS+Cx cells, respectively. These values of J_i were all significantly different from each other, as determined by pairwise comparison. The effect of the magnitude of J_i on the expected kinetics of IIF in cell pairs is discussed in the Supporting Material.

Effect of intercellular junctions on intercellular ice propagation

The effect of intercellular junction protein expression on the rate of intercellular ice propagation (J_p) was examined by computing the cumulative hazard N_p using Eqs. 3–4, based on analysis of the observed state transitions $0^* \rightarrow 1 \rightarrow 2$ (see Fig. 1). Due to the expected role of gap junctions in propagative IIF, the resulting cumulative hazard functions have been separately plotted for MIN6 strains that express the connexin Cx36 (Fig. 7 *A*) and those in which Cx36 expression was knocked-down (Fig. 7 *B*). The magnitude of the propagation rate was estimated by fitting a line to

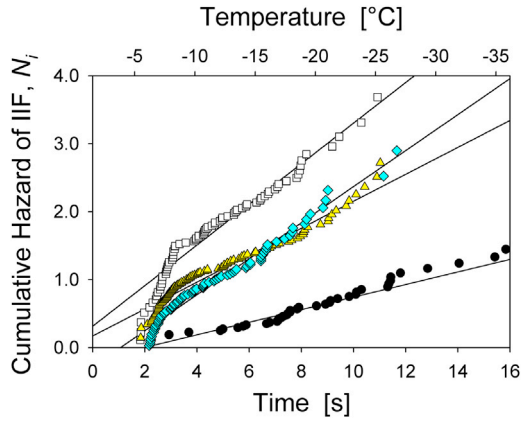

FIGURE 6 Estimated cumulative hazard of cell-cell-interaction-independent IIF (N_i) in cell pairs consisting of wild-type (*circles*), AS (*squares*), AS+Ecad (*triangles*), or AS+Cx strains of MIN6 (*diamonds*). Solid lines represent linear fits to data in the temperature range −6°C to −25°C.

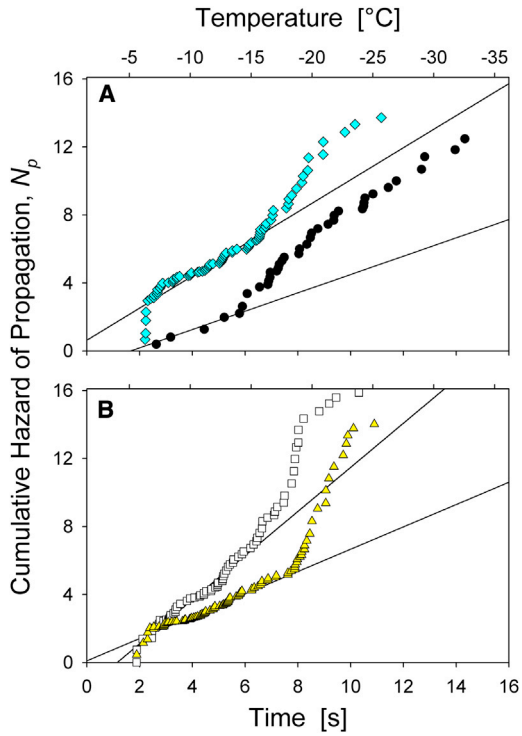

FIGURE 7 Estimated cumulative hazard of intercellular ice propagation (N_p) in cell pairs consisting of wild-type (*circles*), AS (*squares*), AS+Ecad (*triangles*), or AS+Cx strains of MIN6 (*diamonds*). Intercellular ice propagation kinetics is shown for cell strains that express the gap junction protein connexin-36 (*A*), and for the strains lacking connexin-36 (*B*). Solid lines represent linear fits to data in the temperature range −5°C to −15°C.

these data over the temperature range −5 to −15°C, yielding rates of $J_p = 0.54 \pm 0.05\ s^{-1}$ and $0.94 \pm 0.06\ s^{-1}$ for wild-type and AS+Cx, respectively (connexin-expressing strains), and $J_p = 0.66 \pm 0.02\ s^{-1}$ and $1.30 \pm 0.03\ s^{-1}$ for AS+Ecad and AS, respectively (strains with inhibited connexin expression). Analysis of variance on the regression lines showed that these propagation rates were significantly greater than zero for all of the MIN6 strains ($p < 0.001$), including those strains lacking Cx36 expression. In pairwise contrasts, the propagation rate was significantly different in all cases except for the comparison between the wild-type and AS+Ecad strains.

Intercellular ice propagation is expected to manifest as an intracellular crystallization event originating at the cell-cell interface between a previously frozen cell and the unfrozen cell. In cell pairs, the propagative IIF mechanism is only active after the first cell in the pair has frozen; therefore, the probability of observing IIF initiation sites at the cell-cell interface is expected to be higher in the second cell to freeze than in the first cell to freeze. Indeed, as shown in Fig. S3 in the Supporting Material, the proportion of IIF events that originated at the interface was higher for the second freezing event than the first freezing event in all four MIN6 cell variants, and this difference was statistically significant ($p < 0.005$). Thus, beyond the kinetic evidence for intercellular ice propagation shown in Fig. 7, the high-speed imaging technique used here has allowed direct visualization of propagative IIF in the singlet-to-doublet state transition.

DISCUSSION

Cell pairs comprising genetically modified strains of MIN6 were significantly more susceptible to intracellular crystallization during rapid cooling than were the wild-type cell pairs. This is counterintuitive, because the prevailing theory regarding the role of gap junctions in intercellular ice propagation would suggest that the cell pairs expressing Cx36 antisense RNA should exhibit slower IIF kinetics, due to reduced J_p (9,13–15). Furthermore, the increased incidence of IIF in antisense-transfected cells manifested already in the first IIF event in each cell pair (Fig. 2 *B*), which is not dependent on intercellular ice propagation processes (9). A hypothetical explanation for these paradoxical results is that the membranes of the genetically modified MIN6 cells may have lower water permeability than those of wild-type cells, leading to higher water retention (and thus increased supercooling, with concomitant enhancement of IIF kinetics) in the former. To rule out this possibility, we have measured the cell membrane permeability in adherent cultures of wild-type MIN6 (22,23) and the AS strain (24). Predictions of cell dehydration under conditions simulating the present rapid-freezing experiments demonstrated that at temperatures >−15°C, the levels of intracellular supercooling were expected to be comparable in the wild-type and AS strains of MIN6 (24). Therefore, because large discrepancies in the incidence of IIF are evident already in the early stages of freezing (>−15°C), it is unlikely that the observed differences in IIF kinetics between the wild-type and AS strains can be attributed to confounding effects of cellular water transport. Instead, the increased probability of IIF in the genetically modified strains appears to be due primarily to a significant enhancement of the rate of PIP, which was found to have magnitudes four- to eight-fold larger than that of J_{PIP} in wild-type cell pairs.

The PIP process was first described by Stott and Karlsson (10), who identified this phenomenon as a precursor to IIF during the freezing of individual adherent endothelial cells. The form of PIP that was reported by Stott and Karlsson (10) consists of finger-like structures that were observed to grow slowly (~1 μm/ms) inwards, starting at the cell edge; these structures were interpreted as ice dendrites growing into the paracellular space between the basal cell membrane and the glass substrate (10). In the current study, we observed a similar process, manifesting as an increase in opacity at the cell-cell interface over a timescale of ~100 ms. We have interpreted this phenomenon as a variant of PIP, as illustrated in Fig. 8. In particular, we hypothesize that the interfacial darkening events are due to penetration of extracellular ice into the intercellular space, causing ice

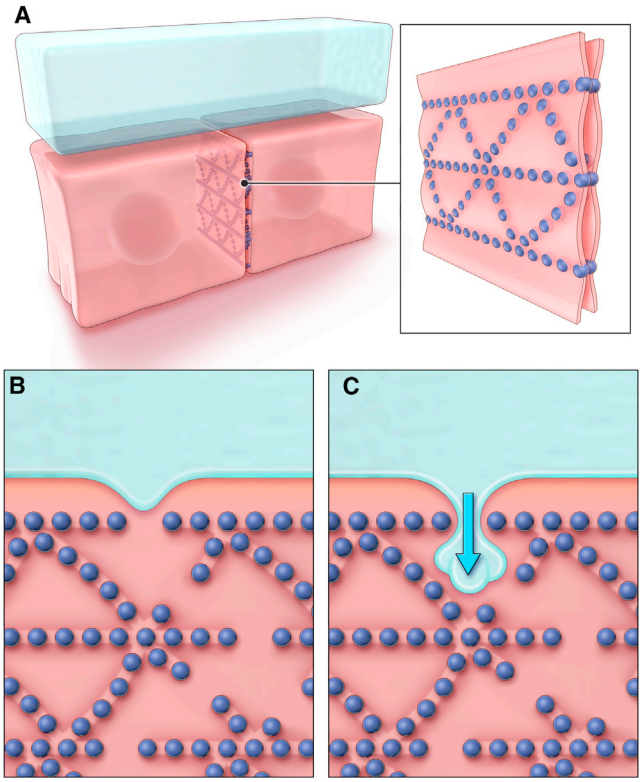

FIGURE 8 Illustration of hypothesized paracellular ice penetration mechanism at the cell-cell interface. (*A*) A cell pair is shown covered by a layer of extracellular ice. Inset is a magnified view of the two interconnected cell membranes, showing a network of junction proteins (depicted as *small spheres*) that are arranged in strands, thus forming paracellular pockets containing unfrozen liquid. (*B*) Cross-sectional view depicting the cell-cell interface, showing a nascent ice protrusion growing from the extracellular ice crystal during cooling. (*C*) When the temperature has fallen below a critical value (T_{PIP}^{max}), the extracellular ice protrusion is able to advance into one of the paracellular pockets, by growing through an opening in the network of intercellular junction proteins (*arrow*). Illustration credit: Scott Leighton.

crystallization in pockets of supercooled liquid trapped between apposing cell membranes. Usually, a sequence of several quick darkening events was observed during PIP, suggesting that multiple distinct domains of supercooled liquid are trapped at the cell-cell interface. We believe that the PIP observations described in this study are analogous to those described by Stott and Karlsson (10), but were localized to the cell-cell interface, rather than the cell-substrate interface. One reason for the different manifestations of PIP is that Stott and Karlsson (10) investigated the freezing of single adherent cell constructs (in which no cell-cell interfaces were created), whereas we have studied IIF in cell pairs.

Based on the hypothesized mechanism of the PIP phenomenon, one would expect the estimated maximum ice penetration temperature ($T_{PIP}^{max} = -5.65°C$) to be consistent with predictions from thermodynamic models of ice growth through pores (14,25). Due to the Gibbs-Thomson effect, reduced temperatures are required to allow ice to penetrate small apertures, because of the curvature imposed on the solidification front in constrained geometries. For paracellular ice growth at the cell-cell interface, the relevant dimension is the separation distance between apposing membranes, which depends on the types of intercellular junction structures present. For example, tight junctions form a network of sealing strands that create interconnections between apposing membranes, but the resulting barriers contain paracellular pores ~0.5 nm in diameter (26); gap junctions are characterized by a membrane separation distance of ~3 nm between neighboring cells (27); adherens junctions exhibit a membrane separation distance of ~25 nm (28). Calculation of the maximum temperature that admits ice growth through a given aperture also requires the contact angle between the ice-liquid interface and the pore wall to be specified. This value is not accurately known, but is thought to be in the range 75–90° (14,25). For the theoretically predicted value of T_{PIP}^{max} to match experimental observations (i.e., $-5.92°C \leq T_{PIP}^{max} \leq -5.41°C$, encompassing the confidence intervals of all MIN6 strains), the contact angle would have to be $88.3 \pm 0.1°$ and $69.1 \pm 1.3°$ for ice penetration through paracellular apertures associated with tight junctions and gap junctions, respectively (see the Supporting Material). In contrast, the membrane separation distance associated with adherens junctions is too large to inhibit ice penetration below −2.9°C, even if the contact angle is 0°. Because the observed values of T_{PIP}^{max} were significantly lower than −2.9°C, one may conclude that the upper-bound temperature for PIP is affected by tight junctions and/or gap junctions, but not adherens junctions. Moreover, considering that the value of the threshold temperature was not very sensitive to connexin expression levels in the different cell strains, the most likely barriers to PIP in our two-cell constructs were the tight junction pores.

Further evidence supporting the hypothesized mechanism of PIP at cell-cell interfaces (Fig. 8) can be obtained by examining the effect of intercellular junction protein expression on the kinetics of PIP, at temperatures below the thermodynamic barrier T_{PIP}^{max}. In particular, the PIP rate constant (J_{PIP}) as well as the total incidence of PIP were found to be significantly lower in wild-type cells than in each of the genetically modified strains. In terms of intercellular junction protein expression, an important difference between these cell strains is that the wild-type cells express the tight junction protein occludin, whereas none of the genetically modified cells expresses occludin at detectable levels (16,17). Because occludin is important for proper function of tight junctions (29), reduced occludin expression may increase the number of defects in the tight junction strands, thus facilitating PIP. This is consistent with the observed increase in the frequency of PIP for the genetically modified MIN6 strains. Furthermore, the rate of PIP in antisense-transfected strains with restored expression of Cx36 (AS+Cx) or E-cadherin (AS+Ecad) was not reduced

compared to the original AS strain, indicating that junction proteins other than connexin and E-cadherin are responsible for the PIP phenomenon in MIN6 cells.

In our experiments, PIP events at the cell-cell interface typically preceded and colocalized with IIF initiation, suggesting a causative relationship between PIP and IIF. Stott and Karlsson (10) also observed a spatiotemporal correlation between PIP and IIF, and postulated that PIP was involved in the IIF mechanism in adherent cells. Moreover, similar ice-cell interactions were reported by Berger (30), who described so-called "aggressive" extracellular ice crystals that were observed to invade tissue via paracellular pathways just before IIF initiation. There are several possible mechanisms by which paracellular ice growth may initiate IIF. For example, ice in the paracellular space may enable surface-catalyzed nucleation at the site of ice-membrane contact (31). Alternatively, the growth of paracellular ice crystals may cause mechanical strain in the cell membrane, possibly leading to membrane failure and attendant growth of ice into the supercooled intracellular compartment. Another possibility that should be considered is that paracellular ice crystals may inoculate the intracellular volume via preexisting membrane pores, such as aquaporins (32) or unpaired connexon channels (33).

If PIP at cell-cell interfaces triggers IIF in the adjoining cells, then the resultant IIF events will be correlated in time. This is important, because experimental observations of a temporal correlation between IIF events in spatially contiguous cells have commonly been interpreted as evidence of intercellular ice propagation (8,11–14). However, as demonstrated in Fig. S2, the PIP process also causes a spatio-temporal correlation of IIF events in cell pairs, even in the absence of intercellular ice propagation. Thus, published cryomicroscopy observations that have previously been attributed to propagative IIF should be revisited in the context of the proposed PIP model, because it is possible that the incidence of propagative IIF has been overestimated. It is also noteworthy that all intercellular ice propagation studies in the literature have used conventional video technology to image IIF at sampling rates <30 Hz (e.g., (9, 13–15)), which is insufficient for direct observation of intracellular crystallization (10). In contrast, we have now visualized intracellular ice growth pathways in the singlet-to-doublet transition using high-speed imaging technology, revealing that the IIF initiation sites for this state transition were preferentially located at the cell-cell interface (see Fig. S3), which is consistent with the intercellular ice propagation hypothesis. Moreover, by analyzing our cryomicroscopy data in the context of a Markov chain model, we confirmed that intercellular ice propagation does occur in MIN6 cells (i.e., the cell pair's two IIF events exhibited temporal correlations that could not be attributed to the coordinating effects of PIP at the cell-cell boundary), and that the associated rate constant J_p was nonzero for all four cell strains.

The most common explanation for intercellular ice propagation is that the underlying mechanism is ice growth through gap junction pores (9,13,14). In particular, Irimia and Karlsson (9) observed a significant reduction in the rate of propagation in micropatterned HepG2 cell pairs after treatment with a connexon disruptor, implicating gap junction intercellular channels in the propagative crystallization process. However, in the MIN6 strains investigated here, expression of Cx36 (in wild-type and AS+Cx cells) paradoxically correlates with a reduction in the intercellular ice propagation rate (compared to AS cells). Furthermore, E-cadherin may also play an inhibitory role in propagative IIF, as evidenced by the high magnitude of J_p in the AS strain (which lacks E-cadherin) compared to wild-type, and the finding that the value of J_p in the AS+Ecad strain (with restored E-cadherin expression) was reduced to a magnitude similar to that of the wild-type strain. Evidently, the dependence of the intercellular ice propagation phenomenon on the architecture of the cell-cell interface is more complex than previously appreciated, and further work will be required to fully elucidate the mechanisms of IIF in tissue constructs.

CONCLUSIONS

Our results shed additional light on the mechanisms of cryoinjury during tissue freezing, by identifying and characterizing an intermediate step (viz., extracellular ice penetration into supercooled paracellular domains at the cell-cell interface) in the IIF pathway for multicellular systems. The evidence suggests that PIP occurs via ice growth through nanoscale apertures in tight junction strands that seal the paracellular spaces at the boundary between neighboring cells, and that such PIP events create a precursor (activated) state that simultaneously enhances the probability of IIF in both adjoining cells. The observed kinetics of IIF initiation and spatial patterns of ice crystal growth in MIN6 cell pairs were consistent with a three-step mechanism of intracellular freezing, in which the first IIF event is caused by the PIP process, and the second IIF event may be triggered either by the paracellular ice or by propagation of intracellular ice from the frozen neighbor cell. Theoretical analysis revealed that although PIP-associated IIF events are correlated with each other (and may therefore masquerade as propagative IIF even when $J_p = 0$), intercellular ice propagation does occur in MIN6 cell pairs. Whereas many researchers have attributed intercellular ice propagation to growth of ice through gap junction channels, we did not observe a reduction in the rate of propagation after downregulation of the junctional protein connexin-36, thus contradicting the prevailing theory of propagative IIF. Future studies are required to better understand the role of different intercellular junction structures in the mechanisms of intercellular ice propagation as well as PIP-associated IIF initiation. Nonetheless, this work illustrates the utility of genetic

engineering techniques and stochastic modeling in mechanistic investigations of tissue cryoinjury.

SUPPORTING MATERIAL

Four figures, three movies, reference (34) and supporting analysis are available at http://www.biophysj.org/biophysj/supplemental/S0006-3495(13)01076-X.

The authors are grateful to Professor Paolo Meda of the University of Geneva for providing the wild-type and genetically modified MIN6 cells.

This work was supported by the National Science Foundation under award No. CBET-0954587 (to J.O.M.K.). Fellowship support (for A.Z.H.) was provided by the National Science Foundation, Howard Hughes Medical Institute, the Medtronic Foundation, and the George Family Foundation.

REFERENCES

1. Karlsson, J. O. M., and M. Toner. 1996. Long-term storage of tissues by cryopreservation: critical issues. *Biomaterials.* 17:243–256.
2. Rajotte, R. V. 1999. Islet cryopreservation protocols. *Ann. N. Y. Acad. Sci*. 875:200–207.
3. McGann, L. E., J. Kruuv, and H. E. Frey. 1972. Repair of freezing damage in mammalian cells. *Cryobiology.* 9:496–501.
4. Armitage, W. J., and B. K. Juss. 1996. The influence of cooling rate on survival of frozen cells differs in monolayers and in suspensions. *Cryo Lett*. 17:213–218.
5. Zieger, M. A. J., E. E. Tredget, and L. E. McGann. 1996. Mechanisms of cryoinjury and cryoprotection in split-thickness skin. *Cryobiology.* 33:376–389.
6. Oegema, Jr., T. R., L. B. Deloria, …, J. L. Lewis. 2000. A simple cryopreservation method for the maintenance of cell viability and mechanical integrity of a cultured cartilage analog. *Cryobiology.* 40:370–375.
7. Liu, B., and J. J. McGrath. 2006. Effects of two-step freezing on the ultra-structural components of murine osteoblast cultures. *Cryo Lett*. 27:369–374.
8. Acker, J. P., A. Larese, …, L. E. McGann. 1999. Intracellular ice formation is affected by cell interactions. *Cryobiology.* 38:363–371.
9. Irimia, D., and J. O. M. Karlsson. 2002. Kinetics and mechanism of intercellular ice propagation in a micropatterned tissue construct. *Biophys. J*. 82:1858–1868.
10. Stott, S. L., and J. O. M. Karlsson. 2009. Visualization of intracellular ice formation using high-speed video cryomicroscopy. *Cryobiology.* 58:84–95.
11. Stuckey, I. H., and O. F. Curtis. 1938. Ice formation and the death of plant cells by freezing. *Plant Physiol*. 13:815–833.
12. Brown, M. S. 1980. Freezing of nonwoody plant tissues. IV. Nucleation sites for freezing and refreezing of onion bulb epidermal cells. *Cryobiology.* 17:184–186.
13. Berger, W. K., and B. Uhrík. 1996. Freeze-induced shrinkage of individual cells and cell-to-cell propagation of intracellular ice in cell chains from salivary glands. *Experientia.* 52:843–850.
14. Acker, J. P., J. A. W. Elliott, and L. E. McGann. 2001. Intercellular ice propagation: experimental evidence for ice growth through membrane pores. *Biophys. J*. 81:1389–1397.
15. Irimia, D., and J. O. M. Karlsson. 2005. Kinetics of intracellular ice formation in one-dimensional arrays of interacting biological cells. *Biophys. J*. 88:647–660.
16. Calabrese, A., M. Zhang, …, P. Meda. 2003. Connexin 36 controls synchronization of Ca^{2+} oscillations and insulin secretion in MIN6 cells. *Diabetes.* 52:417–424.
17. Calabrese, A., D. Caton, and P. Meda. 2004. Differentiating the effects of Cx36 and E-cadherin for proper insulin secretion of MIN6 cells. *Exp. Cell Res*. 294:379–391.
18. Miyazaki, J., K. Araki, …, K. Yamamura. 1990. Establishment of a pancreatic β cell line that retains glucose-inducible insulin secretion: special reference to expression of glucose transporter isoforms. *Endocrinology.* 127:126–132.
19. Karlsson, J. O. M. 2011. An improved method for quantifying intracellular ice formation kinetics when multiple competing mechanisms are active. *Cryobiology.* 63:329–330.
20. Aalen, O. 1978. Nonparametric inference for a family of counting processes. *Ann. Stat*. 6:701–726.
21. Aalen, O. O., Ø. Borgan, and H. K. Gjessing. 2008. Survival and Event History Analysis: A Process Point of View. Springer, New York, NY.
22. Higgins, A. Z., and J. O. M. Karlsson. 2010. Analysis of solution exchange in flow chambers with applications to cell membrane permeability measurement. *Cell. Mol. Bioeng*. 3:269–285.
23. Higgins, A. Z., and J. O. M. Karlsson. 2012. Comparison of cell membrane water permeability in monolayers and suspensions. *Cryo Lett*. 33:96–107.
24. Higgins, A. Z., and J. O. M. Karlsson. 2013. Effect of intercellular junction protein expression on water transport during freezing of MIN6 cells. *Cryobiology.* 67:248–250.
25. Mazur, P. 1965. The role of cell membranes in the freezing of yeast and other single cells. *Ann. N. Y. Acad. Sci*. 125:658–676.
26. Watson, C. J., M. Rowland, and G. Warhurst. 2001. Functional modeling of tight junctions in intestinal cell monolayers using polyethylene glycol oligomers. *Am. J. Physiol. Cell Phys*. 281:C388–C397.
27. Sosinsky, G. E., and B. J. Nicholson. 2005. Structural organization of gap junction channels. *Biochim. Biophys. Acta. Biomembr.* 1711:99–125.
28. Zheng, K., M. Trivedi, and T. J. Siahaan. 2006. Structure and function of the intercellular junctions: barrier of paracellular drug delivery. *Curr. Pharm. Des*. 12:2813–2824.
29. Cummins, P. M. 2012. Occludin: one protein, many forms. *Mol. Cell. Biol*. 32:242–250.
30. Berger, W. K. 2004. Ice can penetrate invertebrate tissues via paracellular pathways. *Cryo Lett*. 25:139–146.
31. Toner, M., E. G. Cravalho, and M. Karel. 1990. Thermodynamics and kinetics of intracellular ice formation during freezing of biological cells. *J. Appl. Phys*. 67:1582–1593.
32. Matsumura, K., B. H. Chang, …, L. Chan. 2007. Aquaporin 7 is a β-cell protein and regulator of intraislet glycerol content and glycerol kinase activity, β-cell mass, and insulin production and secretion. *Mol. Cell. Biol*. 27:6026–6037.
33. Goodenough, D. A., and D. L. Paul. 2003. Beyond the gap: functions of unpaired connexon channels. *Nat. Rev. Mol. Cell Biol*. 4:285–294.
34. Karlsson, J. O. M. 2004. Theoretical analysis of unidirectional intercellular ice propagation in stratified cell clusters. *Cryobiology.* 48:357–361.